ELSEVIER

Polymer 42 (2001) 7117–7126

polymer

www.elsevier.nl/locate/polymer

The microestructure of polyethylene foams produced by a nitrogen solution process

O. Almanza[a], M.A. Rodríguez-Pérez[b,*], J.A. de Saja[b]

[a]*Departmento Física, Universidad Nacional de Colombia, Santafe de Bogota, Colombia*
[b]*Departamento de Física de la Materia Condensada, Facultad de Ciencias, Universidad de Valladolid, 47011 Valladolid, Spain*

Received 9 October 2000; accepted 1 February 2001

Abstract

An experimental study on the cellular structure and polymer morphology of a collection of polyethylene foams produced by a nitrogen solution process is presented in this work. Scanning electron microscopy (SEM) was used to characterise the cellular structure. Raman spectroscopy, wide-angle X-ray diffraction (WAXD), differential scanning calorimetry (DSC), dynamic mechanical analysis (DMA) and SEM were utilised to analyse the polymer morphology. The experimental results showed that the polymer morphology of the solid phase, which comprises the cell walls of the foams is different to that observed in continuous polymers. Moreover, the final polymer morphology of a given foam depends on the cellular structure of the material. © 2001 Elsevier Science Ltd. All rights reserved.

Keywords: Polyolefin foams; Scanning electron microscopy; Dynamic mechanical analysis

1. Introduction

Closed cell polyolefin foams are two phase materials in which contiguous air bubbles are entrapped in a macromolecular phase. These heterogeneous materials have found a wide range of applications in different market sectors as, for example, construction, packaging, buoyancy, automotive, medical, etc. Due to this reason, the control, optimisation and design of the physical properties of these materials are important steps in the development of materials with improved properties and lower cost.

Several studies have been conducted on the structure property relationships for closed cell foams [1–4]. It is widely accepted that the physical properties of a given foam depend on many factors [1,2]. A typical functional dependency would be

$$X = X(\rho, \mathrm{CC}, \mathrm{CS}, \mathrm{PM}, \mathrm{GE}, \text{ etc.}) \quad (1)$$

where X is any physical property, ρ, the foam density, CC, the chemical composition, PM, the polymer morphology and GE is the kind of gas enclosed.

Nowadays, there are more or less detailed studies about the eftect of the density and chemical composition on the physical properties [1,2]. However, the effect of the cellular structure and polymer morphology has not been completely undertaken yet.

One approach to materials design is to develop suitable theoretical models (without adjustable parameters), which allows predicting the physical properties of interest in terms of the main microscopic characteristics of the materials and in terms of the physical properties of the constituent materials. By using these models, the properties could be estimated without producing such materials, and the best combination of microscopic characteristics to improve the tested properties could be deduced.

Different authors have approached the mechanical and thermal properties of foams [1,2,5–10]. In order to apply the existent models it is necessary to know the properties of the polymer which comprises the cell walls of the foams. For semicrystalline materials, these properties are not known and it is assumed that the properties of the same polymer crystallised in a solid sheet can be used instead. However, the polymer in the foam crystallises in exceptional conditions, that is, in the presence of a gas and in very thin cell walls (these cell walls are usually thinner than 2 μm, which is smaller than the typical dimensions of the spherulites in a solid sheet). Therefore, it should be expected that the solid polymer in the cell walls could have different morphology and consequently different properties.

Bearing the previous ideas in mind, an experimental study on the cellular structure and polymer morphology of polyethylene foams produced by a nitrogen solution process

* Corresponding author.
E-mail addresses: marrod@fmc.uva.es (M.A. Rodríguez-Pérez).

PII: S0032-3861(01)00107-0

Table 1
Main characteristics of the foams under study. ρ is the foam density, L is the thickness

Product code	ρ (kg/m^3)	Apparent colour	L ($\times 10^{-2}$ m)
LD15	16.7	White	1.12
LD18	22.5	White	0.96
LD24	24.6	White	1.02
LD29	30.7	White	1.11
LD33	32.0	White	1.10
LD33(1)	32.5	White	1.08
LD50CN	52.3	Black	1.04
LD60	58.5	Green	1.02
LD70B	69.5	Black	1.10
Solid LDPE	910	White	0.93

is presented in this work. Scanning electron microscopy (SEM), Raman spectroscopy, differential scanning calorimetry (DSC), wide-angle X-ray difraction (WAXD) and dynamic mechanical analysis (DMA) are used to characterise the foams.

2. Materials

The product code, measured density (ρ), apparent colour and thickness of the materials under study are summarised in Table 1. All the materials are based on low-density polyethylene (LDPE). The black foam (LD70B) presented a low content of black carbon in its composition (approximately 2% by wt.). The LD50CN foam is an especial grade designed for applications where a higher electrical conductivity is necessary. This material is a blend of LDPE and carbon black with a high content of this last material (10–12% by weight). The main characteristic of the solid sheet that was employed to manufacture the foams is also included in the same table.

These foamed samples are cross-linked closed cell polyolefin foams manufactured by a high-pressure nitrogen gas solution process, and have been kindly provided by ZoteFoams Plc. (Croydon, U.K.). In this process, a polyolefin is compounded with a peroxide curing agent and extruded as a thick sheet which is passed trough a hot oven to effect cross-linking (gel content was approximately 40% for all the foams). The characterised solid sheet was taken from this step of the process. Slabs are cut from the extruded sheet and placed in an autoclave where they are subjected to high pressure (several hundred bars) of nitrogen gas at temperatures above the polymer softening point. Under these conditions, the nitrogen dissolves into the polymer. At the end of the solution stage and after cooling, the pressure is reduced to zero gauge. The slabs, now containing nitrogen gas for expansion, are then placed under low pressure in a second autoclave and again heated above the polymer melting point. Release of the pressure then results in full expansion. Finally, the slabs are taken out of the second autoclave and cooled to room temperature. All the foams are subjected to similar cooling conditions.

3. Experimental

3.1. Density

Density measurements were carried out on the basis of Archimedes principle, using the density determination kit designed for the AT261 Mettler balance.

3.2. Scanning electron microscopy

SEM was used to assess the type of cellular structure, the cell size distribution, the mean cell size, the mean cell wall thickness and the mass fraction in the struts. For this purpose, cross-sections of the foams were microtomed at low temperature to provide a smooth surface, which after vacuum coating with gold, was examined by SEM using a JEOL JSM-820 microscope.

Each micrograph was analysed by obtaining data from 10 reference lines. The cell size distribution was obtained by recording the distance between pairs of cell walls along the reference lines. Magnification was taken into account by using the appropriate factor calculated from the Magnification factor. About 400 cells were analysed for each foam, this quantity was enough to obtain a representative population of the cellular structure. A previous work has demonstrated that the method presented above is equivalent to the image analysis method used for other authors [11].

Each cell size distribution was characterised by means of the mean value (ϕ_m), normalised standard deviation (NSD) and asymmetry coefficient (AC) defined as follows [12].

$$\phi_m = \sum_i m_i f_i, \tag{2}$$

$$\mathrm{NSD} = \frac{\left(\sum_i (m_i - \phi_m)^2 f_i\right)^{1/2}}{\phi_m}, \tag{3}$$

$$\mathrm{AC} = \frac{\sum_i (m_i - \phi_m)^3 f_i}{\mathrm{NSD}^3 \phi_m^3}, \tag{4}$$

where n_i represents the number of cells with a size between a_i and b_i, n is the total number of analysed cells, $m_i = (a_i + b_i)/2$ and $f_i = n_i/n$.

A total of three micrographs were randomly taken over each specimen and subjected to cell size analysis. The 95% confidence error of these three measurements was approximately $\pm 6\%$ of the average value for the mean cell size, and $\pm 10\%$ for the NSD and the AC.

The result obtained by using Eq. (2) was multiplied by 1.62 to take into account the relationship between the

average measured length of the randomly truncated cells and the real diameter of the cell (ϕ) [13].

Foams usually present anisotropic properties. In general the cells have a higher size in the parallel direction to the foaming direction. Therefore, it is necessary to measure the cell size distribution for each one of the three principal directions of the sheets. The degree of anisotropy can be characterised by the ratio between the larger and the smaller cell size (anisotropy ratio (AR)) [14].

In order to obtain a more complete characterisation of the cellular structure two additional parameters are necessary: the mean cell wall thickness (ξ) and the mass fraction in the struts (f_s).

The thickness of thirty cell walls, which were randomly chosen along the foam, was measured directly in the microscope screen. The average value of the previous thicknesses was considered as the mean cell wall thickness of the foams. The 95% confidence interval of these measurements was approximately ±8% of the average value.

Finally, the fraction of mass in the struts was obtained by means of the method proposed by Kuhn [15], measuring through four micrographs taken randomly over each specimen. The 95% confidence error of these measurements was ±8% of the average value.

3.3. Differential scanning calorimetry

Characteristic thermal properties were studied by means of a Mettler DSC30 differential-scanning calorimeter, previously calibrated with indium. The weights of the samples were approximately 2.5 mg. On the one hand, to obtain the crystallinity and melting point of the samples experiments were performed between −40 and 135°C at 10°C/min. On the other hand, to study the possible differences between the crystallisation of the solid polymer in a solid sheet or in a foam non-isothermal crystallisation experiments were carried out. Before each cooling, the samples were heated at 135°C for 4 min in order to erase any previous thermal history. The measurements were performed from 135 to −40°C at the following cooling rates: 1, 2, 5, 10 and 20°C/min.

These experiments were performed on the original foams and on solid sheets produced from the foams by compression in a two plate press at 160°C and 300 bars for 30 min.

The melting point (T_m) was taken as the minimum of the melt peak in the enthalpy curve. The crystallinity (χ_c) was calculated from the DSC curve by dividing the measured heat of fusion by the heat of fusion of a 100% crystalline material (288 J/g for low density polyethylene) [16].

The non-isothermal crystallisation processes were studied following the method developed by Dobreva and Gutzow [17] for the study of the crystallisation kinetics of molten polymers in the presence of nucleating agents. The relationship proposed by these authors is the following

$$\log q \approx \text{const} - \frac{B}{2.3\Delta T^2}, \tag{5}$$

where q is the rate of crystallisation, ΔT is equal to $T_m - T_p$, with T_m the melting temperature and T_p the crystallisation temperature of the samples.

The possible differences between the crystallisation process in the foams and in the solid sheets can be evaluated by using the following parameter

$$\varphi = \frac{B^*}{B^0}, \tag{6}$$

where B^0 is the value of B for the solid sheet and B^* is the value of B for the foams.

Thus, from the experimental slopes in the representation $\log q$ versus $1/\Delta T^2$, according to Eq. (5), it is possible to obtain the B values. Finally, by using Eq. (6), the parameter φ can be estimated.

3.4. Etching

The foams were chemically treated, to reveal the crystalline morphology. The permanganate etching method involved the following steps [18].

1. Add 7% potassium permanganate to concentrated sulfuric acid.
2. Treat the specimen for 60 min at 0°C.
3. Etching is stopped, washing the sample in dilute sulfuric acid at 0°C and leaving decant by 10 min, then washing successively with hydrogen peroxide, water and acetone.

After the treatment, the samples were vacuum coated with gold and examined by SEM.

3.5. Wide-angle X-Ray diffraction

The experiments were performed using a Philips PW 1050/71 diffractometer, using Cu K_α radiation. Radial scans intensity (I) versus scattering angle (2θ) were recorded in the continuous mode between the Bragg angles $2\theta = 5$ and 40°.

The samples were cut parallelepiped-shaped 3.5 cm long. From each sheet, two samples were extracted, the first one was parallel to the Y direction, and the second one perpendicular to the previous direction. A chart of how the samples were cut and how the incidence of the X-ray beam on the sample was archived is shown in Fig. 1. These experiments were used to study the orientation of the crystalline phase of the matrix polymer in each foam.

3.6. Raman spectroscopy

Raman spectra were obtained in the very low-frequency range $\Delta\nu < 100\ \text{cm}^{-1}$ where analysis of the longitudinal acoustic mode (LAM) gives information about the crystallite thickness. A SPEX 1403 Raman spectrometer was used. Instrument excitation was provided by the 514.5 nm radiation of a Spectra Physics Ar^+ laser. Laser power was limited to 100 mW to avoid sample heating.

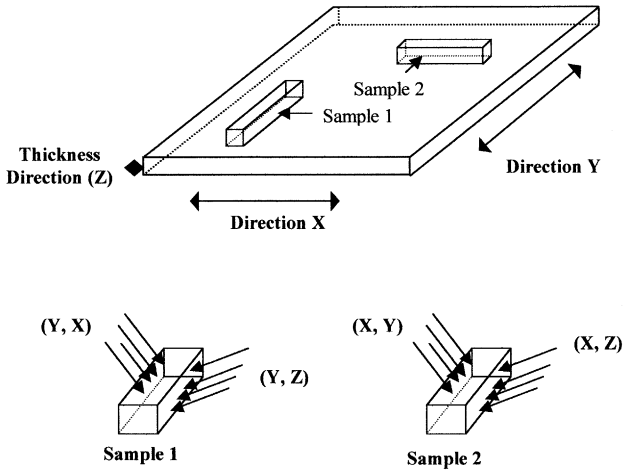

Fig. 1. Samples for the X-Ray diffraction experiments and incidence of the X-Ray beam.

3.7. Dynamic mechanical analysis

The DMA equipment (Perkin–Elmer DMA7) was calibrated according to the recommended procedures using the manufacturer's software. The storage modulus (E'), loss modulus (E''), complex modulus ($E^* = (E'^2 + E''^2)^{1/2}$) and loss tangent or loss factor (tan δ) were obtained in a parallel plate measurement system.

In order to obtain the dynamic mechanical properties as a function of the temperature experiments were performed at 1 Hz frequency, between −40 and 125°C and with a heating rate of 5°C/min. The applied static strain and dynamic strain were chosen in the low strain range (2% static strain and 0.11% dynamic strain). The plate diameter was 10 mm and the test specimens were prepared in a cylindrical shape with the same diameter.

4. Results

The structure of polyolefin foams can be studied, at least, at three different levels (Fig. 2). The cell size distribution and anisotropy of the cellular structure is observed in low magnification micrographs (Fig. 2a). From these micrographs, important parameters as the mean cell size, the anisotropy ratio, the possible rests of foaming agent, and the overall cell shape are usually obtained. In order to obtain a more detailed characterisation of the cellular structure, it is necessary to determine the mean cell wall thickness and the mass fraction in the struts. For this purpose, micrographs with higher magnifications are used (Fig. 2b). Finally, and taking into account the semicrystalline structure of polyolefin foams, it is convenient to consider a third structural level. The shape and size of the constitutive crystals can be estimated by using micrographs as that showed in Fig. 2c. This micrograph corresponds to a cell wall after etching.

In the next sections the structure of the foams object of this work at the three previous levels is presented.

4.1. Cell size distribution and isotropy

The polyolefin foams under study have an isotropic cellular structure, this can be inferred directly from the micrographs of the cellular structure (Fig. 2a) and from the data on Table 2 (AR ≈ 1). Moreover, these materials do not present rests of foaming agent in the cell walls. These two important characteristics, that in general are not true for polyolefin foams produced by extrusion or compression moulding [19], are a consequence of the nitrogen solution process [20].

The data for the mean cell size, NSD and AC are also collected in Table 2. On the one hand, there is no a clear trend for the cell size as a function of the foam density (Fig. 3). On the other hand, the DSN and AC are very similar for all the studied foams. The nitrogen solution process allows controlling the cell size by modifying industrial process parameters as for example the cross-linking degree or the rate at which the pressure is reduced at the end of the solution stage [20]. However, the homogeneity of the distribution and the type of distribution seem to be constant.

4.2. Cell wall thickness, fraction of mass in the struts and average cell shape

The data for the mass fraction in the struts and mean cell thickness are summarised in Table 2. All the foams have a non-negligible mass in the struts. This is a typical result for closed cell polymeric foams, which as has been previously shown strongly affects the mechanical properties [1,2].

The data for the mean cell size and mean cell wall thickness as a function of the density can be observed in Figs. 3a and b. A similar trend as a function of the foam density is observed for both quantities. This result suggests that cell size and cell wall thickness are proportional. The following equation was used to establish the relationship between them.

$$\phi(1 - f_s)\frac{\rho}{\rho_s} = C\xi, \tag{7}$$

where ϕ is the mean cell size, f_s is mass fraction in the struts, ρ is the foam density, ρ_s is the base polymer density, ξ is the mean cell wall thickness and C is a constant that depends on the cell shape, and that, for instance, takes a value of 3.46 for pentagonal dodecahedrons [21].

Our experimental data fits well the previous equation with a value of C of 3.79 (Fig. 4) which seems to indicate that all the foams manufactured by using a nitrogen solution process have cells with the same shapes, which in average, are similar to pentagonal dodecahedrons [20,21].

4.3. Polymer morphology

The values of the crystallinity and melting point for each

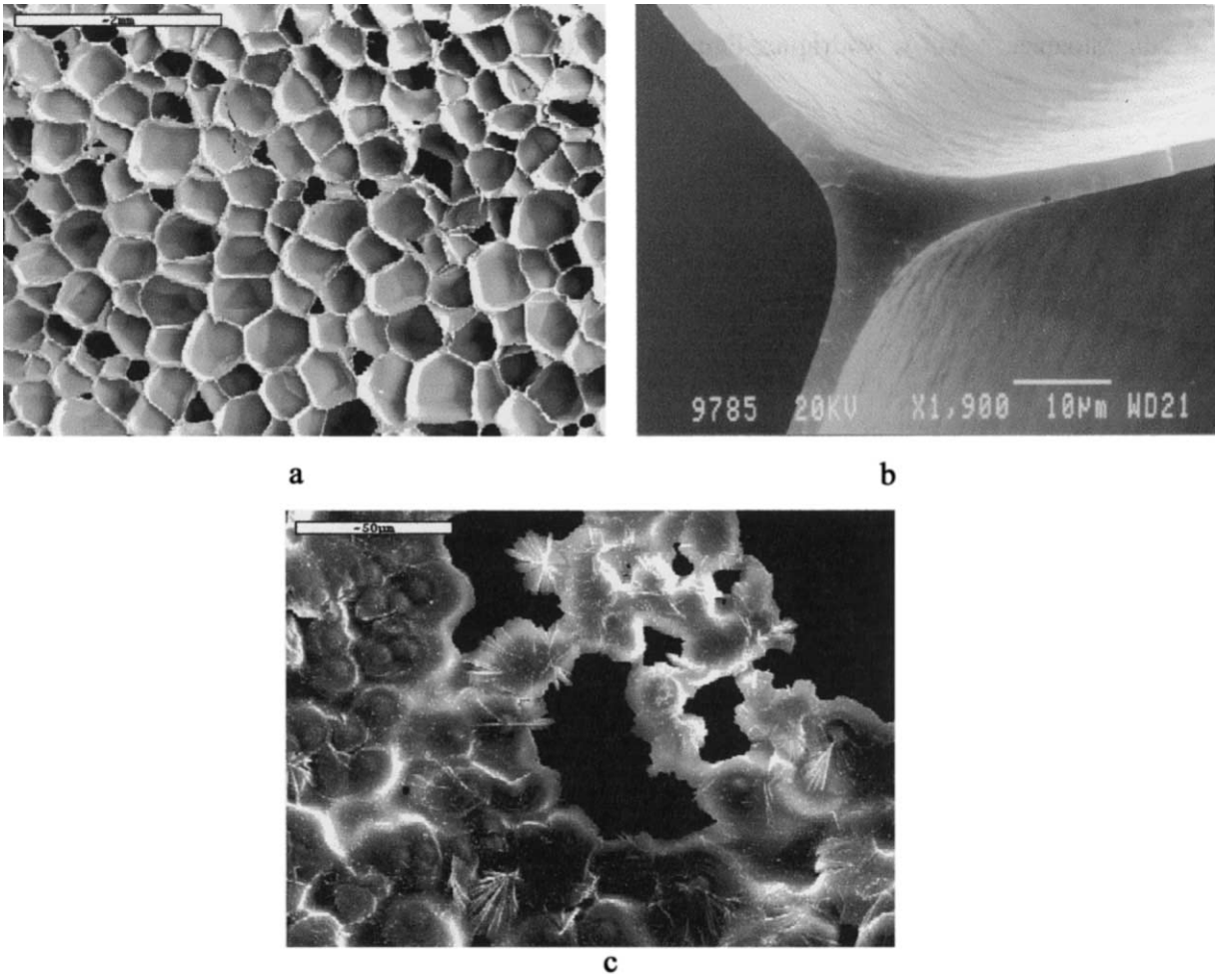

Fig. 2. Three levels of the structure of a polyolefin foam (LD70B): (a) cellular structure; (b) cell walls and struts; (c) morphology of a cell wall after etching.

material are summarised in Table 3. From these data it can be deduced that the solid polymer that comprises the cell walls of these foams has approximately the same melting point and crystallinity (the exceptions are the LD15, LD33 and LD70B foams that were produced from a slightly different LDPE grade). The LD70B and LD50CN foams present an additional black carbon content in their initial formulation. To obtain the crystallinity of these materials it is necessary to introduce a linear correction factor because of the different weight of polymer in these foams. This correction has not been made in the data presented in Table 3, which explain the slightly lower value of the crystallinity of these materials.

Table 2
Microscopic characteristics of the foams under study. ϕ is the mean cell size, NSD is the normalised standard deviation, AR is the anisotropy ratio, AC is the asymmetry coefficient, f_s is the mass fraction in the struts and ξ is the cell wall thickness

Foams	ϕ (μm)	NSD	AR	AC	f_s	ξ (μm)
LD15	313.5	0.43	1.00	0.0021	0.22	1.4
LD18	879.7	0.45	1.01	0.0022	0.21	5.8
LD24	311.9	0.44	1.01	0.0031	0.16	1.9
LD29	528.1	0.46	1.02	0.0029	0.24	4.2
LD33	424.4	0.47	1.00	0.0019	0.28	3.6
LD33(1)	396.9	0.47	0.99	0.0018	0.36	2.5
LD50CN	910.0	0.44	1.00	0.0022	0.22	10.8
LD60	773.4	0.42	1.02	0.0018	0.24	10.3
LD70B	528.1	0.46	1.04	0.0023	0.35	6.0

Some representative examples of the fits of the crystallisation data to Eq. (5) are shown in Fig. 5. Some differences between the observed slopes for the solid polymers and for the foams can be perceived. This is confirmed when the data for the parameter φ are analysed (Table 3). The values are slightly lower than one, which suggests that the crystallisation of the polymer in the foam presents some peculiarities. We will go over this point in the next paragraphs.

Three characteristic images of the polymer after etching are shown in Fig. 6. The first one (Fig. 6a) correspond to the continuous LDPE and the second one to a foam. Well-defined spherulites are observed in the first case, and crystalline unities with a different shape are observed for the foam. If the micrographs are taken in the perpendicular direction to a cell wall, the same structures are found on both sides of the cell wall (Fig. 6c).

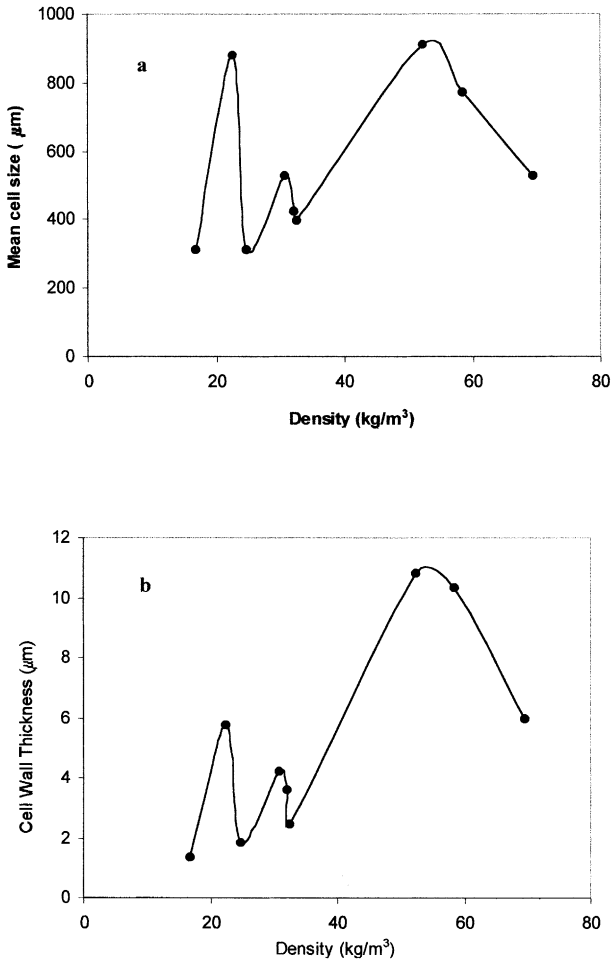

Fig. 3. (a) Mean cell size as a function of density, (b) Mean cell wall thickness as a function of density.

It seems clear that for the foams the crystals start growing from the cell walls surface and they grow towards the centre of the cell walls. Due to this reason the final crystal shape is not spherical and it could be defined as 'spherical caps-shaped crystals'. There are several possibilities to explain this kind of crystallisation.

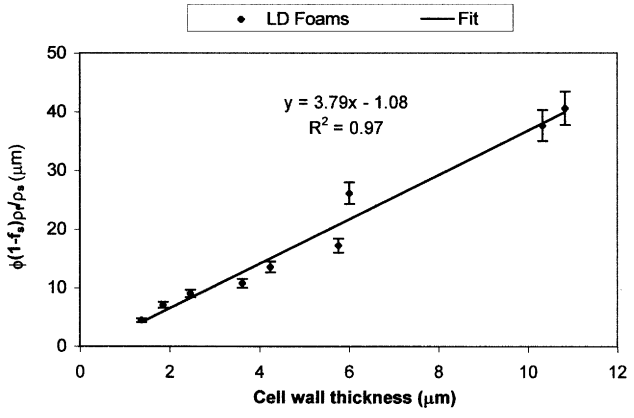

Fig. 4. Fit of the experimental data to Eq. (7).

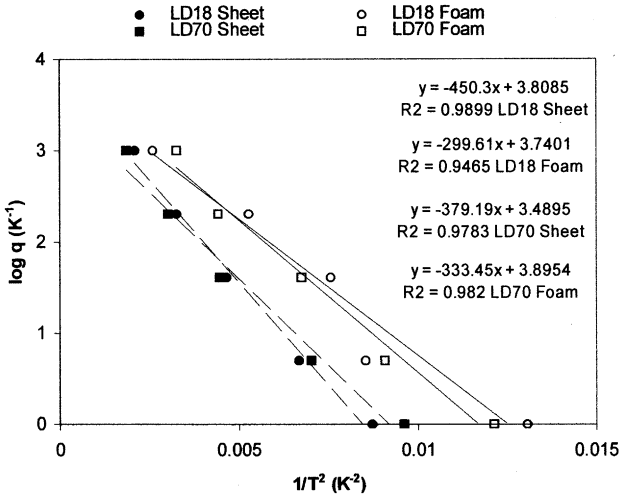

Fig. 5. Fit of the crystallisation data to Eq. (4) for two LD foams and the two solid sheets produced from these foams.

A similar crystal growing has been previously reported in the crystallisation of thin films [22], which satisfied the two dimensionality condition $d/D_s \ll 1$, where d is the thin film thickness and D_s is the typical spherulites diameter. In our case, the cell wall thickness was at least two times lower than the typical diameter of the LDPE spherulites. Therefore, the crystallisation is almost limited to two dimensions. Moreover, previous investigations [23,24] have also shown for inorganic glasses with holes, that it is energetically more favourable that crystals starts growing from the holes surfaces than from the bulk. Finally, another possible explanation would be related with the fact that there is a gas in contact with the polymer surfaces, and this could have some effect on the crystallisation of the matrix.

A remarkable result is obtained if the estimated size of the crystalline forms in the foams is plotted as a function of the foam density (Fig. 7). This curve shows a similar dependence on density than that of the cell size and cell wall thickness. This result suggests that the size of crystals depends, for values under a critical thickness, on the size of the environment where they grow.

Table 3
Thermal characteristics of the foams under study. χ_c is the crystallinity and T_m is the melting point, φ is defined by Eq. (6)

Foams	χ_c (%)	T_m (°C)	φ
LD15	40.6	105.9	0.71
LD18	41.8	108.4	0.67
LD24	43.8	108.6	0.70
LD29	42.9	108.4	0.67
LD33	43.9	105.8	0.78
LD33(1)	41.6	108.6	–
LD50CN	37.0	108.3	–
LD60	42.1	109.0	0.80
LD70B	40.8	106.6	0.88
Solid LDPE	39.2	111.0	1.00

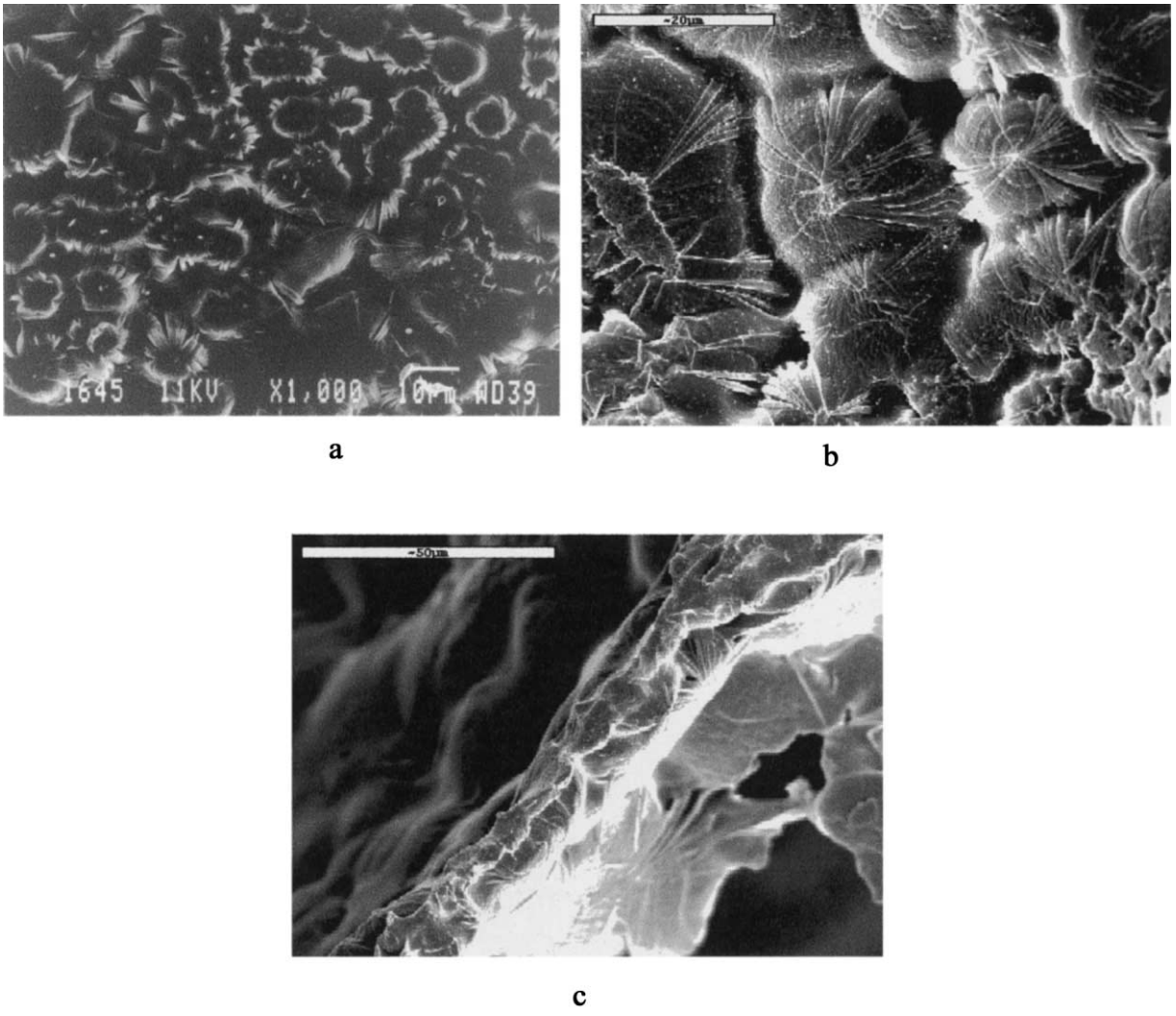

Fig. 6. Crystalline forms: (a) in a solid sheet; (b) in a cell wall (front view); (c) in a cell wall (perpendicular view).

The WAXD data for several materials are presented in Table 4. In order to evaluate the degree of orientation of the crystalline phase, the ratio of the intensity between the (200) to that of the (110) peaks was evaluated [25]. If the data for the solid sheet are considered, it is clear that the previous ratio clearly changes when the X-ray experiment is performed from different directions. Therefore, the solid sheet presents a preferential orientation of their crystalline phase, which is a consequence of the extrusion process in which this sheet is produced. However, the previous change is hardly observed for the low-density foams. Consequently, it is concluded that the preferential orientation observed for the solid sheet decreases during the foam expansion. On the other hand, it is necessary to bear in mind that the expansion produces a biaxial stretching of the cell walls, that it is not detected by X-ray experiments performed for a macroscopic sample. It should be necessary to carry out X-ray experiments on a isolated cell wall in order to characterise its orientation.

Raman spectroscopy was used to obtain structural information of the samples studied. Raman spectra were obtained in the very low-frequency range where analysis of the LAM gives information about the crystalline thickness. The relation between frequency (ν) and the length of the ordered sequence undergoing the vibration is given by [26]

$$L = \frac{m}{2c\Delta\nu}\left(\frac{E_c}{\rho_c}\right)^{1/2}, \tag{8}$$

where m is the mode order, E_c is the elastic modulus in the chain direction, ρ_c is the crystal density (1000 kg/m^3), and c is the velocity of light. A value of $E_c = 2.9\ 10^{11}$ Pa was taken [27].

Fig. 8 shows a typical spectra (LD29). As can be observed three LAM were detected in our experiments. The length, or crystallite thickness, corresponding to the peaks position is given in Table 5. If a given crystal is observed in detail

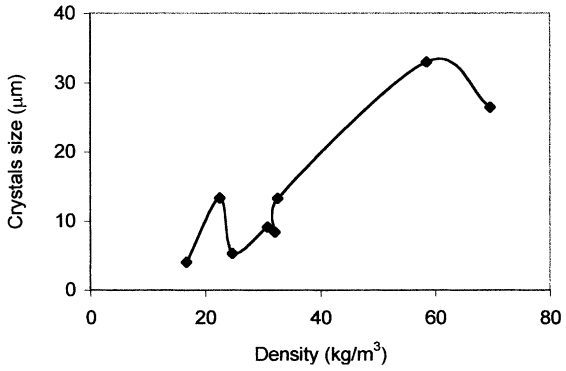

Fig. 7. Crystals size as a function of the density for the LD foams (the LD50CN foam is not included).

(Fig. 9) lamellas of different thicknesses are detected. Moreover, the lamellar thickness does not depend on the foam density and the solid sheet presents the same lamella thickness distribution (Table 5).

The storage modulus (E') and loss factor (tan δ) values as a function of the temperature for the LD foams are presented in Fig. 10a and b. Both curves present the typical behaviour of non-foamed low-density polyethylene. At low temperatures, the β relaxation can be detected as a shoulder in the tan δ curve. In non-foamed PE this relaxation results from motions of chain units located in the interfacial region and its existence is not universal in the different types of polyethylenes, being conditioned by the presence of an interfacial content higher than about 7% [27,28]. Because if this, the β relaxation has been clearly detected, by using dynamic mechanical methods, in branched polyethylene (LDPE) and has not been detected of all in linear polyethylene of medium molecular weight. The α relaxation can be seen at higher temperatures as a wide peak in the tan δ curve. This relaxation has been associated with the crystalline part of the polymer. In fact, the intensity of this relaxation increases as the crystalline content rises for non-foamed polyethylene [27,28] and its position is controlled by the thickness of the lamellae [29].

The storage modulus decreases when the temperature increases and this property is higher for the foams with

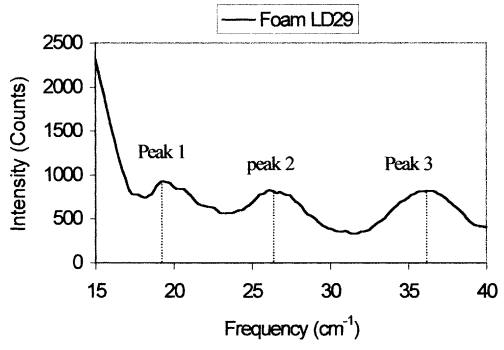

Fig. 8. Typical Raman spectrum of a foam (LD29).

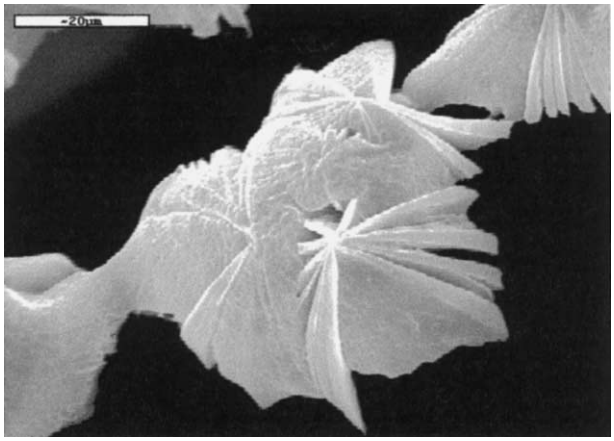

Fig. 9. Typical crystal and lamellar structure observed in a typical foam (LD70B).

higher densities. From the figures it can be deduced that the dynamic mechanical response of these materials depend on density. The complex modulus (E^*) and loss factor as a function of the foam density, for different temperatures, are shown in Fig. 11. The following results can be inferred from the previous figure

(a) In the temperature range under study, the complex modulus increases with density (Fig. 11a). A potential law, $E^* = a\rho^n$, can be utilised to fit the data (Table 6). While at temperatures above 25°C the previous equation fits well the results, deviations are observed at lower temperatures.
(b) While at temperatures above 25°C the loss factor decreases with density, at lower temperatures (in the range of the β relaxation) the shape of the loss factor curve versus density is similar to that of the cell size, cell wall thickness or crystals size versus density (Fig. 11b).

Table 4
WAXD diffraction data for the LDPE solid sheet and for some of the LD foams

LDPE solid sheet	Ratio (200)/(110)	Foams	Ratio (200)/(110)
LDPEXZ	0.34	LD15XZ	0.30
LDPEXY	0.27	LD15XY	0.31
LDPEYX	0.29	LD15YX	0.32
LDPEYZ	0.29	LD15YZ	0.32
		LD18XZ	0.31
		LD18XY	0.32
		LD18YX	0.30
		LD18YZ	0.31
		LD24XZ	0.30
		LD24XY	0.33
		LD24YX	0.32
		LD24YZ	0.34
		LD70XZ	0.28
		LD70XY	0.34
		LD70YX	0.30
		LD70YZ	0.32

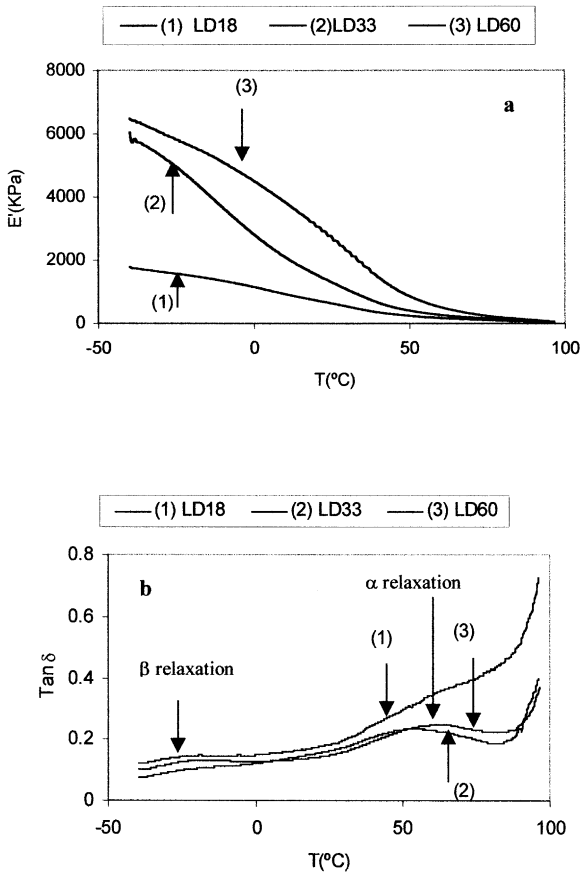

Fig. 10. (a) Storage modulus (E') as a function of the temperature for several LD foams, (b) tan δ as a function of the temperature for several LD foams.

From the previous results some conclusions related with the deformation mechanism can be pointed out. In the low strains range the behaviour of the foams is similar to that of the base polymer from which they were produced [30]. Therefore, the bending of the cell edges and stretching of the cell faces is the first mechanism that controls the response of the foams. The increase of the complex modulus with density is a consequence of the change in the dimensions, and consequently changes of the mechanical resistance, of the elements that build the cellular structure when the density changes.

Table 5
Lamellar thickness obtained from Raman Spectroscopy

Foams	L (Å) 1st Peak	L (Å) 2nd Peak	L (Å) 3rd Peak
LD15	132.9	104.5	77.6
LD18	131.0	102.7	77.6
LD24	125.1	100.6	79.2
LD29	147.4	108.8	78.4
LD33	–	99.6	79.1
LD33(1)	156.9	104.5	77.8
LD50CN	–	–	–
LD60G	132.2	104.9	74.8
LD70B	–	–	–
LDPE solid sheet	141.5	103.4	65.7

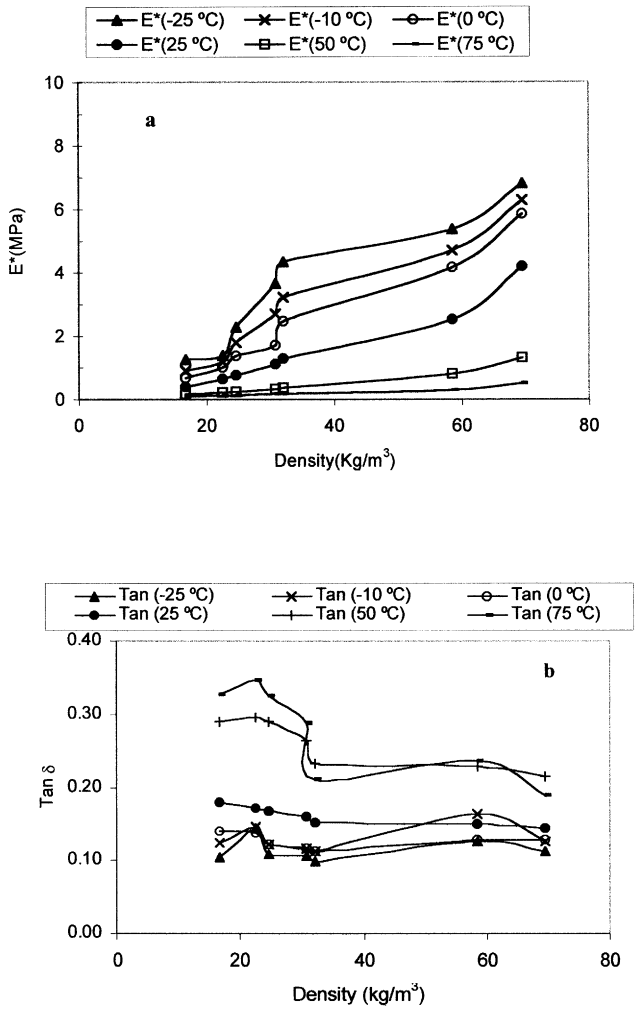

Fig. 11. (a) Complex modulus (E^*) as a function of the density for different temperatures, (b) tan δ as a function of the density for different temperatures.

Moreover, the differences between the loss factor of foams with different densities clearly increase when the temperature rises. This result seems to indicate that the gas pressure inside the closed cells, which also increases with temperature, could be another important mechanism that, especially at high temperatures and low densities, influences on the dynamic mechanical response of closed cell foams [31].

However, at low temperatures (in the β relaxation zone)

Table 6
Values of n, a and R^2

T (°C)	n	a	R^2
−25	1.20	0.78	0.86
−10	1.34	1.00	0.93
0	1.47	1.25	0.97
25	1.58	1.06	0.99
50	1.48	0.24	0.99
75	1.04	0.03	0.94

this last mechanism would play a minor role, consequently the different response of the foams must be understood in terms of a different matrix polymer morphology in each foam, which was observed by SEM.

5. Conclusions

The previous discussion allows obtaining a description of the structure of these materials. On the one hand, it is necessary to emphasise that the materials produced by a high-pressure nitrogen solution process have a closed cell cellular structure in which there is no residues of foaming agent, the cell shape is very similar for foams of different densities and the cells are isotropic. On the other hand, these materials present a matrix polymer with a different morphology to that is observed in the solid sheet from which they are produced. The crystals grow in very different conditions, that is in very thin cell walls, in the presence of a gas and after a expansion process. This result in a completely different morphology, that is mainly characterised by crystals with 'spherical cap shape' and with dimensions directly related to the cell wall thickness. Lamellas of different thicknesses are the constituent of these crystalline forms. It is also important to note that the orientation of the solid sheet almost disappear when the foam is expanded.

Finally, it has been shown that the dynamic mechanical response of the foams at low temperatures depends on the density. This is a consequence, first of the different cellular structure of foams with different densities and second of the different polymer morphology of foams with different cellular structure. The dynamic mechanical properties at low temperatures, zone in which the gas enclosed plays a minor role, depends on the polymer morphology. In fact, this is a consequence of the different morphology and consequently different properties of the matrix in each foam. The same kind of result would probably be observed if other properties are considered.

Different matrix polymer morphology results in different foam properties. As a consequence, the prediction of the properties in terms of the density, cellular structure and properties of a solid polymer is a difficult task

Acknowledgements

Financial assistance from the CICYT (MAT99-0979) is gratefully acknowledged. O. Almanza also thanks COLCIENCIAS (Colombia) for their financial support. We should also like to thank Zotefoams Plc. for supplying the foams.

References

[1] Gibson LJ, Ashby MF. Cellular solids: structure and properties. Oxford: Pergamon Press, 1988.
[2] Hilyard NC, Cunningham A. Low density cellular plastics: physical basis of behaviour. London: Chapman and Hall, 1994.
[3] Klempner D, Frisch C, editors. Polymeric foams. Munich: Hanser, 1991.
[4] Kumar VA, Seeler KA. Cellular and microcellular materials, vol. 53. New York: The American Society of Mechanical Engineers, 1994.
[5] Leach AG. J Phys D: Appl Phys 1993;26:733.
[6] Colishaw PG, Evans JRG. J Mater Sci 1994;29:486.
[7] Williams RJJ, Aldao CM. Polym Engng Sci 1983;23:32.
[8] Bedeaux D, Kapral R. J Chem Phys 1983;79:1783.
[9] Mills NJ, Gilchrist A. Cellular Polym 1997;16:87.
[10] Clutton EQ, Rice GN. Cellular Polym 1992;11:429.
[11] Sims GL, Khumiteekoll C. Cellular Polym 1994;13:137.
[12] Rodríguez-Pérez MA, Alonso O, Duijsens A, de Saja JA. J Polym Sci: Polym Phys Ed 1998;36:2587–96.
[13] ASTM D3576, Annual Book of ASTM Standards, vol. 8 (02). 1994.
[14] Cowin SC. J Mater Sci 1991;26:5155.
[15] Kuhn J, Ebert HP, Arduini-Schuster MC, Büttner D, Fricke J. Int J Heat Mass Transfer 1992;35:1795.
[16] Wunderlich B. Macromolecular physics, vol. 2. New York: Academic Press, 1976. p. 1973.
[17] Dobreva-Veleva A, Gutzow I. J Non Cryst Solids 1993;162:13–25.
[18] Shahin MM, Olley RH, Blisset MJ. J Polym Sci: Polym Phys 1999;37:2279.
[19] Rodríguez-Pérez MA, Duijsens A, de Saja JA. J Appl Polym Sci 1998;68:1237–44.
[20] Almanza OA, Rodríguez-Pérez MA, de Saja JA. Cellular Polym 1999;18:6.
[21] Almanza O, Rodríguez-Pérez MA, de Saja JA. J Polym Sci: Polym Phys 2000;38:993.
[22] Ivanov DA, Nysten B, Jonas AM. Polymer 1999;40:5899.
[23] Schmelzer J, Möller J, Gutozw I, Pascova R, Müller R, Panhorst A. J Non Cryst Solids 1995;183:215.
[24] Schmelzer J, Pascova R, Möller J, Gutzow I. J Non Cryst Solids 1993;162:26.
[25] Carole R, Marianne G, Proceedings of the Eurofillers Conference, Lyon, 1999.
[26] Mizushima S, Shimanouchi T. J Am Chem Soc 1949;17:1320.
[27] Popli R, Glotin M, Mandelker L. J Polym Sci: Polym Phys 1990;28:569.
[28] Alberola N. J Polym Sci: Polym Phys 1984;22:407.
[29] Sinnot KM. J Appl Phys 1966;37:3385.
[30] Rodríguez-Pérez MA, Rodríguez-Llorente S, Saja de JA. Polym Engng Sci 1997;37:959.
[31] Rodríguez-Pérez MA, Saja de JA. Polym Testing 2000;19:115.